Monthly Notices
of the
ROYAL ASTRONOMICAL SOCIETY

MNRAS **486,** 3498–3505 (2019)
Advance Access publication 2019 April 13

doi:10.1093/mnras/stz1071

Gas phase SiO in the circumstellar environment of the recurrent nova T Coronae Borealis

A. Evans,[1]★ Ya. V. Pavlenko,[2,3] D. P. K. Banerjee,[4] U. Munari,[5] R. D. Gehrz,[6] C. E. Woodward,[6] S. Starrfield,[7] L. A. Helton,[8] M. Shahbandeh,[9] S. Davis,[9] S. Dallaporta[10] and G. Cherini[10]

[1]*Astrophysics Group, Lennard Jones Laboratory, Keele University, Keele, Staffordshire ST5 5BG, UK*
[2]*Main Astronomical Observatory, Academy of Sciences of the Ukraine, Golosiiv Woods, Kyiv-127 UA-03680 Ukraine*
[3]*Centre for Astrophysics Research, University of Hertfordshire, College Lane, Hatfield, Hertfordshire AL10 9AB, UK*
[4]*Physical Research Laboratory, Navrangpura, Ahmedabad 380009, Gujarat, India*
[5]*INAF Astronomical Observatory of Padova, I-36012 Asiago (VI), Italy*
[6]*Minnesota Institute for Astrophysics, School of Physics, Astronomy, University of Minnesota, 116 Church Street SE, Minneapolis, MN 55455, USA*
[7]*School of Earth and Space Exploration, Arizona State University, Box 871404, Tempe, AZ 85287-1404, USA*
[8]*USRA-SOFIA Science Center, NASA Ames Research Center, Moffett Field, CA 94035, USA*
[9]*Department of Physics, Florida State University, 77 Chieftan Way, Tallahassee, FL 32306, USA*
[10]*ANS Collaboration, Astronomical Observatory, I-36012 Asiago (VI), Italy*

Accepted 2019 April 8. Received 2019 April 5; in original form 2019 February 20

ABSTRACT

We report the discovery of the diatomic molecule SiO in the gas phase in the environment of the recurrent nova T Coronae Borealis. While some of the SiO is photospheric, a substantial portion must arise in the wind from the red giant component of T CrB. A simple fit to the SiO feature, assuming local thermodynamic equilibrium, suggests a SiO column density of 2.8×10^{17} cm^{-2} and temperature ∼1000 K; the SiO column density is similar to that present in the winds of field red giants. A search for SiO maser emission is encouraged both before and after the next anticipated eruption. We find that the ^{12}C/^{13}C ratio in the red giant is <9, with a best-fitting value of ∼5, a factor ∼18 times lower than the solar value of 89. We find no convincing evidence for the presence of dust in the environment of T CrB, which we attribute to the destructive effects on nucleation sites of hard X-ray emission. When the next eruption of T CrB occurs, the ejected material will shock the wind, producing X-ray and coronal line emission, as is the case for the recurrent nova RS Oph. T CrB is also a good candidate for very high energy γ-ray emission, as first observed during the 2010 outburst of V407 Cyg. We include in the paper a wide variety of infrared spectroscopic and photometric data.

Key words: stars: AGB and post-AGB – circumstellar matter – stars: individual: T CrB – novae, cataclysmic variables – infrared: stars.

1 INTRODUCTION

Recurrent novae (RNe) are a subclass of the cataclysmic variables that consist of a compact component (a white dwarf; WD) and a cool donor star. Depending on the nature of the system, material from the donor star spills over on to the WD via an accretion disc.

Like classical novae, they are the result of a thermonuclear runaway on the surface of the WD. All novae are recurrent but RN eruptions, unlike those of classical novae, recur on a human time-scale (≲100 yr) rather than an astronomical time-scale (Starrfield 2008). Therefore, RNe are defined by the selection effect that they have been observed to undergo more than one eruption.

There is strong evidence that the mass of the WD in RN systems is close to the Chandrasekhar limit (e.g. Thoroughgood et al. 2001). As material from the donor star spills over on to the WD, it is possible that the net flow of matter on to the WD (taking into account any mass lost in eruptions) is positive, the mass of the WD may increase, eventually taking it over the Chandrasekhar limit (e.g. Starrfield et al. 2019).

There are undoubtedly several channels to Type Ia supernova explosions, although none is currently clearly favoured (see Maoz, Mannucci & Nelemans 2014, and references therein). However, should the WD in an RN system gain mass, and it has Carbon–Oxygen composition (Maoz et al. 2014), such RN systems may be

★ E-mail: a.evans@keele.ac.uk

one of the progenitors of Type Ia supernovae (see Munari & Renzini 1992; Maoz et al. 2014). Studying RNe therefore provides us with the opportunity to understand the progenitors of such supernovae, which are a key tool in the determination of the cosmic distance scale and of cosmic large-scale structure (Perlmutter et al. 1997, 1999; Reiss et al. 1998).

RNe are a heterogeneous set of objects but they fall naturally into two types (Anupama 2008): (a) those with long orbital periods (e.g. RS Oph, T CrB, orbital periods of months–years), in which the cool component is a red giant (RG) and (b) those with short orbital periods (e.g. U Sco, T Pyx, orbital periods of hours–days); the cool component in these systems may be a main-sequence dwarf or a subgiant.

2 LONG-PERIOD RECURRENT NOVA SYSTEMS

Four RN systems with long orbital periods are (as of 2019) known, although only T CrB and RS Oph have well-determined orbital periods (227.67 and 455.72 d, respectively; see Anupama 2008); the long orbital periods of the other two (V745 Sco and V3890 Sgr) are inferred from the fact that they have RG secondaries. Such systems are commonly referred to as 'symbiotic binaries'.

In these long-period systems, the RG usually has a wind and, when the RN eruption occurs, the ejecta run into and shock the RG wind. The subsequent deceleration of the ejecta is manifested in the narrowing of emission lines as the eruption proceeds (e.g. Evans et al. 2007a; Munari et al. 2011). Hydrodynamical modelling of this phenomenon has been carried out by Walder, Folini & Shore (2008) for the case of the 2006 eruption of RS Oph, and by Pan, Ricker & Taam (2015) for the 2010 eruption of the symbiotic binary V407 Cyg. The interaction between the ejecta and the wind results in X-ray and non-thermal radio emission, as well as coronal line emission in the optical and infrared (IR); very high energy γ-ray emission – as seen in V407 Cyg (Cheung et al. 2010) – may also be expected (Banerjee et al. 2014).

The outbursts of the long-period systems are very homogeneous, to the extent that the visual light curves of successive eruptions of a given RN are practically indistinguishable (Anupama 2008). They behave like 'fast' novae of the He/N type: the light curves decline at $\sim$0.3 mag d^{-1}, and material is ejected at high velocity, several thousand km s^{-1}. The 2006 eruption of RS Oph was particularly well observed from X-rays to radio (Das, Banerjee & Ashok 2006; Evans et al. 2008; Banerjee, Das & Ashok 2009; Drake et al. 2009; Ness et al. 2009).

3 THE RECURRENT NOVA T CRB

T CrB has undergone eruptions in 1866 and 1946, and there may have been an eruption in 1842 (Schaefer 2010, but see also Schaefer (2013)). The properties of T CrB are discussed in detail by Anupama & Mikoławjeska (1999); an updated account is given by Munari, Dallaporta & Cherini (2016).

Anupama (2008) gives its distance and interstellar reddening as 1.3 kpc and $E(B-V) = 0.15$, respectively. Schaefer (2009) gives a distance of 800 $\pm$ 140 pc, by an average of several independent methods. While there is a parallax for T CrB from the *Gaia* survey (leading to a distance of 825 $\pm$ 33 pc), this may be unreliable because of orbital motion (Schaefer 2018). The reddening is likely somewhat smaller than Anupama's value (see Schlegel, Finkbeiner & Davis 1998; Schlafly & Finkbeiner 2011; Green et al. 2018). According to Green et al., the reddening in the direction of T CrB levels out

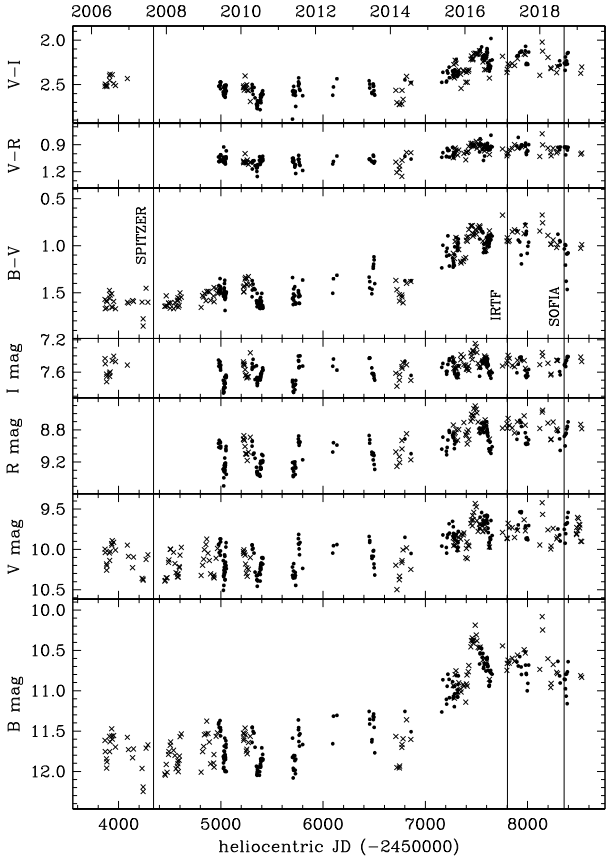

Figure 1. *BVRI* light curves of T CrB covering the *Spitzer*, IRTF, and *SOFIA* observations; the JD times of the *Spitzer*, IRTF, and *SOFIA* observations are indicated. Data from the ANS Collaboration; the different symbols represent data from two separate telescopes, working independently to provide an independent check.

to a value $E(B-V) = 0.07 \pm 0.02$ beyond $\sim$350 pc; Schlafly & Finkbeiner give $E(B-V) = 0.058$, while Schlegel et al. give $E(B-V) = 0.062$. We assume $E(B-V) = 0.06$ here. The reddening is so low that it is a very minor source of uncertainty in our analysis.

The post-1946 photometric evolution is described by Munari et al. (2016), who find evidence for a superactive photometric phase starting in 2015. This is well illustrated in Fig. 1, which draws on data from the Asiago Novae and Symbiotic stars (ANS) collaboration (Munari et al. 2012; Munari & Moretti 2012). The apparent scatter in the light curves is real, and is a consequence of the strong orbital modulation induced by irradiation of the M3III RG secondary by the WD, and ellipsoidal variations due to the RG filling its Roche lobe (Yudin & Munari 1993). The onset of the active state in 2015, which is evident in Fig. 1, was accompanied by significant changes in the X-ray emission (Luna et al. 2017). There is also evidence for flickering activity (Iłkiewicz et al. 2016).

Both the ultraviolet (UV) continuum and emission lines are highly variable (Anupama & Mikoławjeska 1999). Selvelli, Cassatella & Gilmozzi (1992) estimated the UV luminosity to be $\sim$40 L$_\odot$, implying a mass accretion rate on to the WD of $\sim 2.5 \times 10^{-8}$ M$_\odot$ yr^{-1}.

T CrB was detected by *Swift* in 2005 June–October (Kennea et al. 2009); they find that its spectral energy distribution (SED) in the 0.3–150 keV range is well fitted by a single-temperature ($\sim$28 keV) bremsstrahlung model. The absorbing column density is $\sim 21.5 \times 10^{22}$ cm^{-2}, some 400 times larger than the column density expected from absorption in the general interstellar medium.

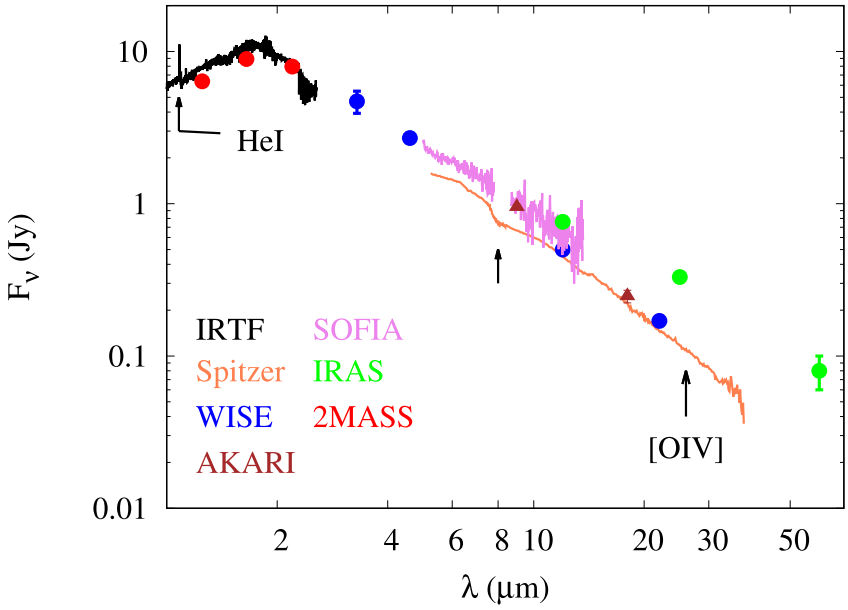

Figure 2. IRTF, *Spitzer* IRS, and *SOFIA* FORCAST spectra of T CrB, with 2MASS, *WISE*, *AKARI,* and *IRAS* photometry superimposed; errors in 2MASS, *WISE*, *AKARI,* and *IRAS* photometry are smaller than points if not visible. The He I $\lambda = 1.083$ μm line is labelled, as is the expected location of the [O IV] $\lambda = 25.89$ μm line. The arrow at 8 μm shows the SiO absorption feature discussed in Section 8.1.

Kennea et al. conclude that the absorption must be intrinsic to T CrB. They also estimate that the mass of the WD in the T CrB system is 1.35 $M_\odot$, concluding that the WD in T CrB is close to the Chandrasekhar limit. This finding is consistent with the $M_{WD} = 1.3$–$2.5\,M_\odot$ derived by Shahbaz et al. (1999), based on modelling the ellipsoidal variations in the IR light curve and assuming an orbital inclination of order 38–46°. Luna, Sokoloski & Mukai (2008) observed T CrB with the *Suzaku* X-ray observatory in 2006 September. They too found that there is a substantial ($\sim 35 \times 10^{22}$ cm^{-2}) circumstellar hydrogen column density.

While symbiotic binaries are known to be soft X-ray sources, T CrB is one of a small number of this class known to be a hard X-ray source (Eze 2014, and references therein); it is likely that the hard X-rays arise at the boundary layer between the WD and the accretion disc (e.g. Kennea et al. 2009).

Recently, Shara et al. (2018) summarized the WD masses and accretion rates for several recurrent and classical novae. For T CrB they give $\sim 1.35\,M_\odot$ for the WD mass and $2.1 \times 10^{-8}\,M_\odot$ yr^{-1} for the accretion rate, suggesting that both parameters are well determined for T CrB.

Luna et al. (2018) recently described *Swift* and *XMM*–Newton observations of T CrB, combined with optical data over a 12 yr period. These data show a marked rise in the optical/UV flux accompanied by a decline in the X-ray flux. Luna et al. ascribe this to a disc instability event, and that the optical brightening is similar to that seen some 8 yr before the 1946 eruption. This is consistent with the analysis by Munari et al. (2016), who suggest that T CrB is due to erupt around 2026. Luna et al. estimate an X-ray absorbing column density of $\sim 6.8 \times 10^{23}$ cm^{-2}, significantly higher than is the case for the earlier X-ray observations (Kennea et al. 2009; Luna et al. 2008).

It is important that the T CrB system is well observed prior to the next eruption so that the evolution of the eruption can be interpreted in an informed manner. In this paper, we present IR observations of T CrB, and report the discovery of gas-phase molecular SiO in absorption, and an estimation of the ^{12}C/^{13}C ratio in the RG component.

4 OBSERVATIONS

4.1 Infrared photometric observations

There are a number of IR photometric observations of T CrB in the public domain.

(i) It is listed as an *IRAS* source by Harrison & Gehrz (1992), who found fluxes (in Jy) of 0.76 ± 0.03, 0.33 ± 0.02, 0.08 ± 0.02 in *IRAS* Bands 1 (12 μm), 2 (25 μm), and 3 (60 μm), respectively; it was not detected in Band 4 (100 μm) to a limit of 0.31 Jy.

(ii) It is detected in the *Wide-field Infrared Survey Explorer* (*WISE*; Wright et al. 2010) survey, with fluxes (in Jy) of 4.70, 2.70, 0.50, and 0.17 in the *WISE* Bands 1 (3.3 μm), 2 (4.6 μm), 3 (12 μm), and 4 (22 μm), respectively (Evans et al. 2014). The *WISE* photometry is fitted by a 4300 K blackbody (Evans et al. 2014), somewhat hotter than the 3500 K expected for a M3III star (Cox 2000).

(iii) T CrB also appears in the 2MASS (Strutskie et al. 2006) survey, with fluxes (in Jy) of 6.37 (*J*), 8.91 (*H*), 7.95 (K_s).

(iv) T CrB is an *AKARI* (Ishihara et al. 2006) source, with flux densities 0.95 ± 0.04 Jy at 9 μm and 0.25 ± 0.02 Jy at 18 μm.

The 2MASS, *WISE*, *AKARI*, and *IRAS* data are plotted in Fig. 2. It is noticeable that the *IRAS* fluxes are significantly higher than those from *WISE*; there is therefore a possibility that T CrB may be variable in the mid-IR on a ∼20 yr time-scale.

4.2 *Spitzer Space Telescope*

T CrB was observed on 2007 August 30 with the *Spitzer Space Telescope* (Werner et al. 2004; Gehrz et al. 2007) InfraRed Spectrograph (IRS; Houck et al. 2004) as part of the *Spitzer* programme PID 40060 (PI A. Evans). The *Spitzer* IRS spectrum, shown in Fig. 2, reveals the Rayleigh–Jeans tail of the RG photosphere; the IRS data are consistent with the *WISE* photometry, indicating that there has been minimal change in the mid-IR between the *Spitzer* (2007) and *WISE* (2011) observations. We note here that both the *Spitzer* and *WISE* data were obtained before the onset of the activity in 2015.

4.3 NASA Infrared Telescope Facility

T CrB was observed with the SpeX spectrograph (Rayner et al. 2006) on the 3 m NASA Infrared Telescope Facility (IRTF) on 2017 February 17.63 UT at spectral resolution of 1200 over the 0.77–2.50 μm region. Details of the observations and data reduction are given in Munari & Banerjee (2018); the IRTF data are included in Fig. 2.

4.4 *SOFIA*

T CrB was observed with the Faint Object IR CAmera for the SOFIA Telescope (FORCAST; Herter et al. 2012, 2013) instrument on the NASA *Stratospheric Observatory for Infrared Astronomy* (*SOFIA*; Young et al. 2012).

The observations were carried out on two separate flights, on 2018 August 24.24 UT (flight F498) and 2018 August 30.22 UT (flight F494), as part of our *SOFIA* Cycle 6 programme to monitor RNe between eruptions (PI A. Evans, proposal ID 06_0096). T CrB was observed with the G063 and G111 grisms, using the 4.7 arcsec × 191 arcsec slit to give spectral resolution $R \simeq 70$. The on-target integration times were 1000 and 3000 s for grisms G063 (flight 498) and G111 (flight 494), respectively. Both observations used the default 2-point chop/nod 'Nod_Match_Chop' mode. We assume that, as the time-interval between the two observations are substantially less than the variations due to orbital modulation, the two spectral segments can be combined.

The *SOFIA* data are included in Fig. 2. It seems that the flux density in the 5–13 μm range was higher in 2018 than it was in 2007, when the *Spitzer* data were obtained; as T CrB is a point source this difference cannot be ascribed to (for example) differences between the instrument parameters between the *Spitzer* IRS and *SOFIA* FORCAST, such as slit width. Indeed, while the *Spitzer* fluxes are consistent with the *WISE* data, the *SOFIA* fluxes are closer to those measured by IRAS in 1983. As we note in Section 5 below, the orbital phase during both the *Spitzer* and the *SOFIA* observations were similar: the flux difference between these observations cannot therefore be attributed to either irradiation of the RG or ellipsoidal variations. It must presumably be due to the increased activity since 2015 (see Fig. 1).

5 ORBITAL PHASE

Fig. 1 shows the *BVRI* light curves over the period covered by the *SOFIA*, *Spitzer* and IRTF observations.

As discussed in Munari et al. (2016), the photospheric temperature of the RG changes by up to a couple of spectral sub-types as a result of the combined effect of orbital aspect and irradiation by the WD companion. The orbital phase of the *Spitzer* observation – as determined from the ephemeris of Kenyon & Garcia (1986) and Fekel et al. (2000) – was 0.985 (i.e. the irradiated side of the RG is hidden from view), while for the IRTF observation it was 0.680 (i.e. the irradiated face of the RG is almost in full view). The orbital phase was 0.123 at the time of the *SOFIA* observation, so again the irradiated face of the RG was not visible.

The binary phase must be accounted for in the modelling.

6 SYNTHETIC SPECTRA

Synthetic spectra for the RG were computed using the WITA6 program (Pavlenko 1997), assuming local thermodynamic equilibrium (LTE), hydrostatic equilibrium and a one-dimensional model atmosphere without sources and sinks of energy. Theoretical synthetic spectra were computed for RG model atmospheres having effective temperatures in the range $T_{\rm eff} = 3000$–4000 K, and gravities $\log g$ in the range 0–3 with a gravity step $\Delta \log g = 1.0$. A microturbulence velocity of 2 km s^{-1} was assumed.

In addition to atomic lines, molecular lines of H_2O, TiO, CrH, VO, CaH, ^{12}CO, and ^{13}CO are included (see Pavlenko, Jones & Longmore 2003; Pavlenko et al. 2008, for details). Computations were performed for the 1D SAM12 model atmospheres (Pavlenko 2003). The goodness of fit is determined in the usual way by minimizing the *S* parameter (Pavlenko et al. 2003, 2008). Direct comparison of the SAM12 and MARCS (Gustafsson et al. 2008) model atmospheres shows good agreement in their temperature structures ($\lesssim$50 K), despite the differences in the adopted abundance scales.

We discuss the near-IR and mid-IR separately.

7 THE NEAR-IR

7.1 The effects of irradiation

An initial best fit to the near-IR SED yields a $T_{\rm eff} = 3600$ K, $\log g = 3$, and solar abundances, as shown in Fig. 3 (top panel).

However, we know that the irradiated face of the RG was in almost full view at the time of the IRTF observation, and this must be taken into account (see Pavlenko et al. 2016, for an application of this to the RG in RS Oph). We find that an improved fit is obtained if some allowance is made for the irradiation of the RG by the WD. The model flux is now

$$F_{\rm total} = a\, F_{\rm SAM12} + (1 - a)\, B_\lambda(T_{\rm BB})\,,$$

where $F_{\rm total}$, $F_{\rm SAM12}$ and $B_\lambda(T_{\rm BB})$ are the total model flux, the flux from the SAM12 synthetic spectrum and the contribution of a blackbody at temperature $T_{\rm BB}$, respectively; $(1 - a)$ effectively represents the fraction of the visible RG hemisphere that is irradiated by the WD. We explored values of $T_{\rm BB}$ of 5000, 7350, 10 000, and 12 500 K, and a in the range $0 \geq a \geq 0.9$, with increments of 0.1, and $0.9 \geq a \geq 1$, with increments of 0.01.

An improved fit is obtained to the near-IR SED with the same SAM12 synthetic spectrum, and $T_{\rm BB} = 5000$ K and $a = 0.93$ (see bottom panel of Fig. 3). The calculated $F_{\rm total}$ fits the spectrum well, including the deep TiO bands in the red; individual atomic lines are also well reproduced. We note in Fig. 3 that there is an apparent excess in the synthetic spectrum compared with the data around 1.6 μm. The former is effectively for a 'normal' RG, in which the H^- continuum is prominent, whereas the RG in T CrB is in a binary with a WD. The dissociation energy of the H^- ion is 0.75 eV, and we suggest that it does not survive, especially on the irradiated side of the RG, thus leading to a reduction in the observed flux around 1.6 μm.

7.2 The ^{12}C/^{13}C ratio

The first overtone CO bands are clearly present in the IRTF spectrum (see Fig. 4); indeed inspection shows that both ^{12}CO and ^{13}CO isotopologues are present. The fit discussed in Section 7.1, including irradiation, applied to the 2 μm region of the spectrum, shows that the first overtone CO absorption is best fitted with ^{12}C/^{13}C $\simeq 5$ (see Fig. 4), a factor ∼18 times lower than the solar value of 89 (Wilson 1999; Coplen et al. 2002; Clayton & Nittler 2004); however, all the spectral resolution allows us to conclude is that ^{12}C/^{13}C $\lesssim 9$. Even with this limit the ^{12}C/^{13}C ratio is lower than that found in the RG of RS Oph (^{12}C/^{13}C $= 16 \pm 3$; Pavlenko et al. 2010). Indeed,

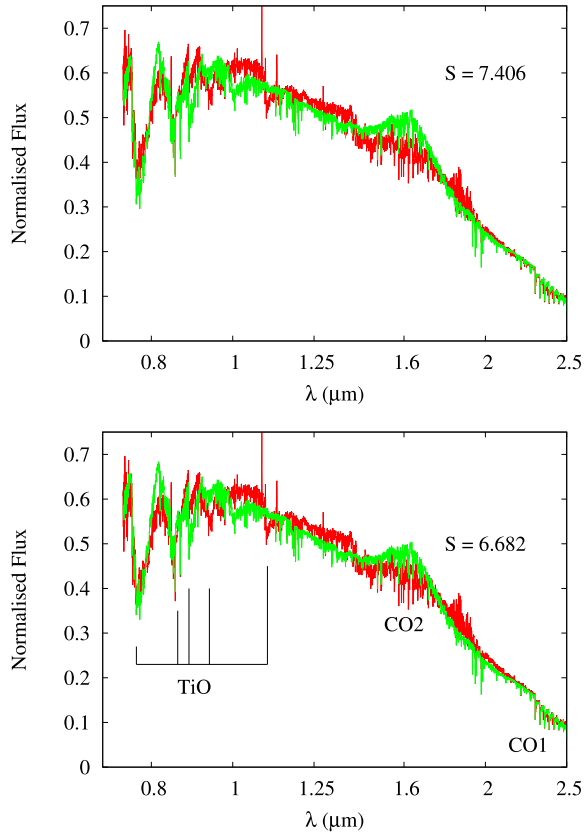

Figure 3. Top: Fit of synthetic spectrum (green) to the observed near-IR SED of T CrB (red); no irradiation. Bottom: Fit of the synthetic spectrum together with irradiation by a blackbody as discussed in the text. Wavelength scale is logarithmic to highlight the fit at the shorter wavelengths. In both cases the parameter *S* represents the goodness of fit. Bottom frame includes identification of some prominent molecular absorptions; CO1 and CO2 are the first and second overtone CO bands, respectively. Note that the atmospheric transmission is poor around 1.4 and 1.8 μm.

this ratio in T CrB is towards the extreme low end of the $^{12}C/^{13}C$ ratio recently found observationally in RGs in the open cluster NGC 6791 (Szigeti et al. 2018), and is much lower than that predicted (∼20) by the post-dredge up evolution scenario (Charbonnel 1994).

8 THE MID-IR

8.1 SiO in the RG

Clearly visible in the *Spitzer* spectrum is a weak absorption feature at around 8 μm (see Figs 2 and 5). To highlight this feature we have fitted a power-law function

$$f_\nu = A\,\lambda^{\alpha}$$

to the continuum on either side of the feature (see Fig 5); the fit shown is for $\alpha = -1.71 \pm 0.02$. The wavelength of maximum absorption and the profile of this feature is consistent with the $\Delta\upsilon = 1$ fundamental transition in gas-phase SiO, which has long been known in the spectra of late giants and supergiants (see e.g. Geballe, Lacy & Beck 1979; Decin et al. 2004; Sloan et al. 2015). We therefore attribute the feature in T CrB to absorption by gas-phase SiO and, in view of the nature of the system, the SiO must originate in the M3III component.

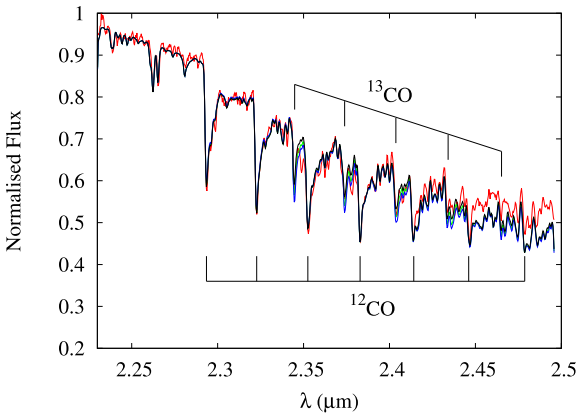

Figure 4. Fit of model fluxes, including irradiation, to the observed fluxes (red) across the CO first overtone band with $^{12}C/^{13}C = 5$ (green); other curves are for $^{12}C/^{13}C = 9$ (black) and $^{12}C/^{13}C = 3$ (blue). The $\Delta\upsilon = 2$ band-heads are identified.

SiO is added to the synthetic spectrum used in Section 7.2 to model the IRTF spectrum, except that the irradiation by the WD is 'switched off' in view of the relative orientations of the WD, RG, and observer (see Section 5). We take data for SiO (energy levels, partition function, etc.) from the *Exomol* project (Barton, Yurchenko & Tennyson 2013; Hill, Yurchenko & Tennyson 2013), which are appropriate for a zero pressure gas (i.e. pressure broadening is not taken into account); only the isotopologue $^{28}Si^{16}O$ is included.

We find that, for solar abundances, the optical depth in the photospheric SiO bands does not fully match the *Spitzer* observations: *additional absorption is required to account for the depth of the feature*. We might make ad hoc adjustments to the abundances of Si and/or O in the RG atmosphere to enhance the SiO abundance, and hence strengthen the SiO fundamental feature. However, such action would have adverse effects on other (atomic) features in the spectrum where the agreement between synthetic and observed spectra is good.

We conclude that the additional absorption must arise in the RG wind.

8.2 SiO in the RG wind

We therefore amend the calculated flux to

$$F_\lambda = F_{\rm SAM12}\ \exp(-\tau_{\rm SiO})\,,$$

where $\tau_{\rm SiO}$ is the optical depth due to SiO in the RG wind. For simplicity the absorbing material is placed in a plane-parallel slab between the RG and the observer, and the only free parameters are the column density of SiO and the temperature of the gas in the wind. We find that the entire SiO feature is well fitted by the photospheric component, but with an additional component having $T \simeq 1000$ K and a column density of SiO $N(\rm SiO) = 2.9 \times 10^{17}$ cm^{-2}; this is comparable to the SiO column density in field RGs (Ohnaka 2014).

If the absorbing column reported by Kennea et al. is mostly in the form of H, we estimate that $N(\rm SiO)/N(H) \sim 1.3 \times 10^{-6}$; the value in M-type Asymptotic Giant Branch (AGB) stars is in the range $\sim$[2–50] $\times\ 10^{-6}$ (González Delgado et al. 2003), so its value in the wind of T CrB is very much at the lower end of this range.

The binding energy of SiO (8.26 eV) is substantially lower than that of CO (11.09 eV), so CO will be better able to survive in the 1000 K RG wind than SiO. Indeed, the low value of $N(\rm SiO)/N(H)$ deduced above may be related to the hostile environment in which

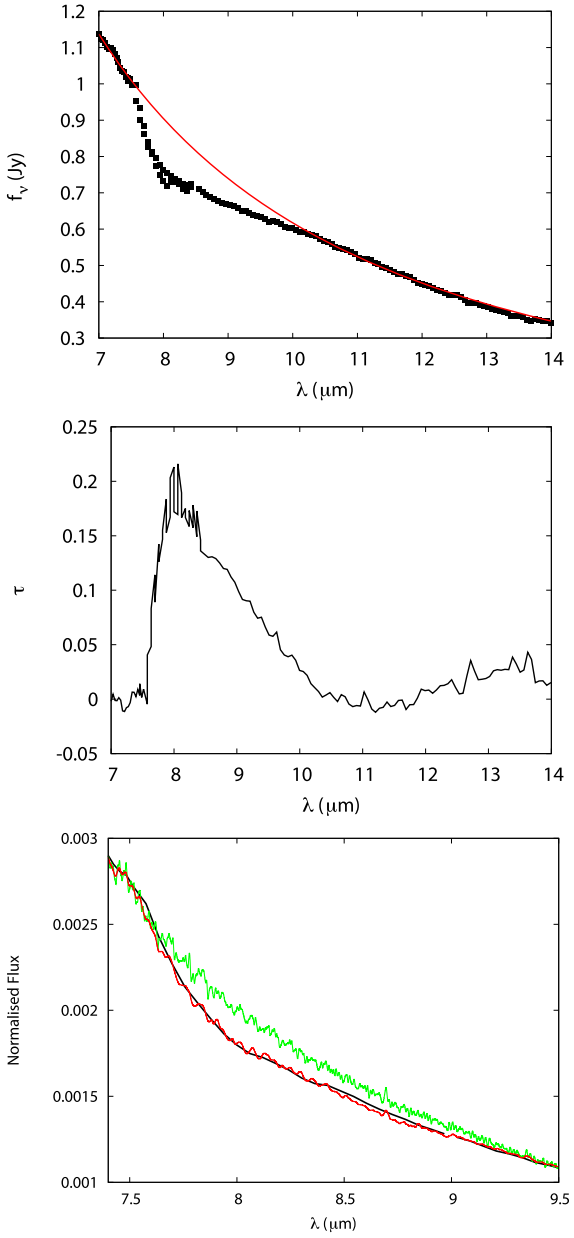

Figure 5. Top: Power-law fit to the continuum around 8 μm as discussed in the text. Middle: Optical depth in SiO feature. Bottom: 8 μm feature in T CrB (black). Green curve is contribution of photospheric SiO. Red curve is the combined effect of absorption by SiO in the RG photosphere, with an additional contribution from SiO in the RG wind. The SiO column density is 2.9×10^{17} cm^{-2}, the wind temperature is 1000 K. See the text for details.

the SiO is located in T CrB. As the column density of CO in the RG photosphere is $\simeq$30 × greater than that of SiO, we estimate that the column density of CO in the wind should be $\sim 9 \times 10^{18}$ cm^{-2}. A spectrum in the region of the CO fundamental at 4.67 μm would therefore be particularly valuable because we predict that, as is the case with the SiO fundamental, the CO fundamental will be deeper than that corresponding to the first overtone[1] discussed in Section 7.2.

[1]We note that, at ∼1000 K, the relative populations of the $\upsilon = 1$ and $\upsilon = 2$ vibrational levels in CO is ∼27: 1, so there is negligible contribution to the observed first overtone CO absorption from the wind.

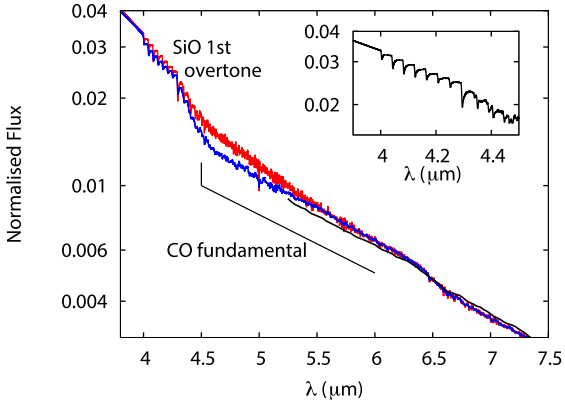

Figure 6. Spectrum in the region of the CO fundamental and SiO first overtone. Black line: *Spitzer* IRS data. Red line: RG photosphere only. Blue line: RG photopshere plus column density of 2.9×10^{17} cm^{-2} (SiO) and 9×10^{18} cm^{-2} (CO). Approximate extent of the ^{12}CO fundamental is indicated. Inset shows detail around SiO first overtone.

There is some evidence that the CO fundamental is indeed deeper than that expected from a pure photospheric contribution (see Fig. 6, in which the SAM12 model is plotted to fit the region of the CO fundamental absorption). The CO fundamental is expected to cover the wavelength range ∼4.2–6 μm, but unfortunately our Spitzer data only start at 5.2 μm. It can still be seen however that a contribution from CO, over and above photospheric, is needed to explain the depth of the CO fundamental in the Spitzer data. As discussed above, we believe that this additional CO originates in the RG wind and, based on the SAM12 fit in Fig. 6, we estimate that the column density of CO in the wind is $\sim 9 \times 10^{18}$ cm^{-2}. A spectrum covering the entire wavelength range covered by the CO fundamental would be valuable to tie down this number. A search for the corresponding SiO first overtone absorption (band-heads in the wavelength range 4.02–4.13 μm) would also be helpful, in particular high-resolution spectroscopy to determine isotopic ratios; the predicted profiles of the SiO first overtone are shown in Fig. 6.

We note here that a search for SiO maser emission from T CrB in the $J = 1 \rightarrow 0$, $\upsilon = 1$ transition at 43.122 GHz yielded a non-detection (Blair & Dickinson 1977). However, Deguchi et al. (2011) detected SiO maser emission, from both the $J = 1 \rightarrow 0$, $\upsilon = 1$ (43.122 GHz) and $J = 1 \rightarrow 0$, $\upsilon = 2$ (42.821 GHz) transitions in V407 Cyg several weeks after its 2010 eruption. They found dramatic and complex changes in the SiO maser emission from the Mira component as the post-eruption shock swept through the Mira wind. In view of our detection of SiO in the RG wind of T CrB, an attempt to detect maser emission is highly desirable, both before and after the anticipated RN eruption. Such observations would provide a rare opportunity to study the dynamics of the nova eruption.

8.3 No dust in the T CrB system

We see from Fig. 2 that, if there is a 'conventional' 9.7 μm silicate feature in the *Spitzer* IRS spectrum of T CrB in either emission or absorption, its peak relative to the adjacent continuum is <20 mJy (3σ); we can place a similar limit on the absorption in/emission by various polymorphs of silica (SiO_2), which peak in the wavelength range ∼8.4–10 μm (Koike et al. 2013). In stark contrast to the case of RS Oph (see Evans et al. 2007b; Woodward et al. 2008; Rushton et al. 2014), there is no evidence for silicate dust in the T CrB system.

Why is gas-phase SiO detectable in the wind of T CrB whereas the 9.7 μm solid state silicate feature is essentially absent, while the silicate feature is in emission in RS Oph? On the face of it the two systems are similar, with giant secondaries, similar orbital periods and massive WDs.

The conventional picture of dust formation in AGB stars (see e.g. Habing & Olofsson 2004) is that simple molecules (such as TiO, CO, SiO in the case of oxygen-rich systems) are present in the wind in a region just above the RG atmosphere. Above this region is the dust-forming layer, where oxygen-rich species, such as silicates, and aluminium and magnesium oxide solids, form and grow. However, a necessary condition for the formation and growth of dust grains is the presence of nucleation sites: if such sites are not present then dust cannot form in the wind.

In the case of T CrB and RS Oph, a key aspect in which they seem to differ is in their X-ray emission. RS Oph is relatively X-ray faint, in contrast to T CrB (see Mukai 2008). Moreover, as noted in Section 3, T CrB is a hard X-ray source whereas RS Oph is not. We suggest that the layer in the RG wind of T CrB, where nucleation sites would usually be expected to form, is persistently exposed to hard radiation from the WD, thus preventing the formation of nucleation sites.

8.4 The [O IV] fine structure line

Apart from the He I $\lambda = 1.0833$ μm triplet (see Fig. 2), there appear to be no particularly strong emission lines in the IR spectrum of T CrB. Weak features seen are those of O I $\lambda = 0.8446$, 1.1287 μm, and Pa-γ and Pa-β at 1.0940 and 1.2818 μm, respectively (see Munari & Banerjee 2018).

A notable absentee is the [O IV] fine structure line at $\lambda = 25.89$ μm (Fig. 2), which is ubiquitous in mature classical novae (e.g. Evans & Gehrz 2012; Helton et al. 2012, and references therein), and is present in the IR spectrum of the RN RS Oph (Evans et al. 2007b; Rushton et al. 2014). We set a 3σ upper limit of 6.2 mJy on the peak flux density in the [O IV] line.

We suppose that this line is quenched by collisional de-excitation by electrons. At ∼1000 K – the temperature deduced for the SiO-bearing material (see Section 8.2) – the critical electron density below which radiative de-excitation dominates collisional de-excitation for the [O IV] line is 4.64×10^3 cm^{-3}; at 10^4 K, the critical density is 9.94×10^3 cm^{-3} (see table 4 of Helton et al. 2012). The absence of the [O IV] line in T CrB implies therefore that the electron density in the wind must be at least $\sim 5 \times 10^3$ cm^{-3}.

It is not trivial to convert a lower limit on electron density to a hydrogen column density; however, this lower limit on the electron density is not inconsistent with the high column density required by the X-ray observations.

9 CONCLUDING REMARKS

We have presented IR photometry and spectroscopy of the recurrent nova T CrB. We summarize our conclusions as follows:

(i) we have found the SiO fundamental – commonly seen in evolved stars – in absorption at 8 μm. The observed strength of the feature is such that a significant proportion must arise in the RG wind. The deduced SiO column density in the wind is similar to that seen in the winds of field RG stars;

(ii) a search for SiO maser emission from T CrB, both before and after its next eruption, is desirable;

(iii) we predict that the CO fundamental will also be stronger than is necessary to account for photospheric absorption, and that the column density of CO in the wind is $\sim 9 \times 10^{18}$ cm^{-2};

(iv) the ^{12}C/^{13}C ratio in the RG is $\simeq$5, very much at the low end of that expected on the basis of post-dredge up evolution;

(v) there is no evidence of silicate dust in the environment of T CrB's RG, in contrast to the case of RS Oph. This is likely a consequence of the stronger, and harder, X-ray source in the T CrB binary compared with that in RS Oph.

When the next eruption of T CrB does occur, the ejected material will run into and shock the RG wind, so we might expect that the evolution of the eruption will, superficially at least, resemble those of the eruptions of RS Oph, with strong X-ray emission and strong coronal line emission; indeed coronal lines were prominent in the optical spectrum of T CrB during the 1946 eruption (Bloch, Fehrenbach & Tcheng 1946; Bloch & Tcheng 1953). A list of IR coronal lines is given in table 2 of Evans & Gehrz (2012); many of these lines will be accessible to the FORCAST instrument on *SOFIA*.

Moreover, the recent detection of classical novae as γ-ray sources (Ackermann et al. 2014), and the nature of the T CrB system, strongly suggests that T CrB will likely be a γ-ray source when it erupts (Banerjee et al. 2014; Metzger et al. 2014, 2015).

Clearly, suitable observations of T CrB when it does eventually erupt are highly desirable, and we hope that this work will provide an impetus to further observations of T CrB in quiescence as we approach the next eruption.

ACKNOWLEDGEMENTS

We thank the anonymous referee, Dr Tom Geballe and the editor for their help with improving the original version of this paper.

Based in part on observations made with the NASA/DLR Stratospheric Observatory for Infrared Astronomy (*SOFIA*). *SOFIA* is jointly operated by the Universities Space Research Association, Inc. (USRA) under NASA contract NNA17BF53C, and the Deutsches SOFIA Institut (DSI) under DLR contract 50 OK 0901 to the University of Stuttgart.

This publication makes use of data products from the Two Micron All Sky Survey, which is a joint project of the University of Massachusetts and the Infrared Processing and Analysis Center/California Institute of Technology, funded by the National Aeronautics and Space Administration and the National Science Foundation. It also makes use of data products from the *Wide-field Infrared Survey Explorer*, which is a joint project of the University of California, Los Angeles, and the Jet Propulsion Laboratory/California Institute of Technology, funded by the National Aeronautics and Space Administration.

The IRTF is operated by the University of Hawaii under contract NNH14CK55B with the National Aeronautics and Space Administration. We are very grateful to David Sand for making possible the IRTF observation.

The research work at Physical Research Laboratory is supported by the Department of Space, Government of India. RDG was supported by NASA and the United States Air Force. SS is grateful for partial support from NASA and *HST* grants to ASU. CEW was supported by NASA *SOFIA* resources under contracts from USRA. UM is partially supported by the PRIN-INAF 2017 'Towards the SKA and CTA era: discovery, localization and physics of transient sources' (PI M. Giroletti).

REFERENCES

Ackermann M. et al., 2014, Science, 345, 554
Anupama G. C., 2008, in Evans A., Bode M. F., O'Brien T. J., Darnley M. J., eds, ASP Conf. Ser. Vol. 401, RS Ophiuchi (2006) and the Recurrent Nova Phenomenon. Astron. Soc. Pac., San Francisco, p. 31
Anupama G. C., Mikołajewska J., 1999, A&A, 344, 177
Banerjee D. P. K., Das R. K., Ashok N. M., 2009, MNRAS, 399, 357
Banerjee D. P. K., Joshi V., Venkataraman V., Ashok N. M., Marion G. H., Hsiao E. Y., Raj A., 2014, ApJ, 785, L11
Barton E. J., Yurchenko S. N., Tennyson J., 2013, MNRAS, 434, 1469
Blair G. N., Dickinson D. F., 1977, ApJ, 215, 552
Bloch M., Tcheng M.-L., 1946, Ann. Astrophys., 9, 157
Bloch M., Tcheng M.-L., 1953, Ann. Astrophys., 16, 73
Charbonnel C., 1994, A&A, 282, 811
Cheung C. C., Donato D., Wallace E., Corbet R., Dubus G., Sokolovsky K., Takahashi H., 2010, Astron. Telegram 2487.
Clayton D. D., Nittler L. R., 2004, ARA&A, 42, 39
Coplen T. B. et al., 2002, Pure Appl. Chem., 74, 1987
Cox A. N., 2000, Allen's Astrophysical Quantities. Springer-Verlag, Berlin
Das R., Banerjee D. P. K., Ashok N. M., 2006, ApJ, 653, L141
Decin L., Morris P. W., Appleton P. N., Charmandaris V., Armus L., Houck J. R., 2004, ApJS, 154, 408
Deguchi S., Koike K., Kuno N., Matsunaga N., Nakashima J.-I., Takahashi S., 2011, PASJ, 63, 309
Drake J. J. et al., 2009, ApJ, 691, 418
Evans A. et al., 2007a, MNRAS, 374, L1
Evans A. et al., 2007b, ApJ, 671, L157
Evans A., Gehrz R. D., 2012, BASI, 40, 213
Evans A., Bode M. F., O'Brien T. J., Darnley M. J., 2008, in Evans A., Bode M. F., O'Brien T. J., Darnley M. J., eds, ASP Conf. Ser. Vol. 401, RS Ophiuchl i (2006) and the Recurrent Nova Phenomenon. Astron. Soc. Pac., San Francisco.
Evans A., Gehrz R. D., Woodward C. E., Helton L. A., 2014, MNRAS, 444, 1683
Eze R. N. C., 2014, MNRAS, 437, 857
Fekel F. C., Joyce R. R., Hinkle K. H., Skrutskie M. F., 2000, AJ, 119, 1375
Geballe T. R., Lacy J. H., Beck S. C., 1979, ApJ, 230, L47
Gehrz R. D. et al., 2007, Rev. Sci. Inst., 78, 011302
González Delgado D., Olofsson H., Kerschbaum F., Schöier F. L., Lindqvist M., Groenewegen M. A. T., 2003, A&A, 411, 123
Green G. M. et al., 2018, MNRAS, 478, 651
Gustafsson B., Edvardsson B., Eriksson K., Jørgensen U. G., Nordlund Å., Plez B., 2008, A&A, 486, 951
Habing H. J., Olofsson H., eds, 2004, Asymptotic Giant Branch Stars, Astronomy and Astrophysics Library. Springer, Berlin
Harrison T., Gehrz R. D., 1992, AJ, 103, 243
Helton L. A. et al., 2012, ApJ, 755, 37
Herter T., Adams J. D., De Buizer J. M. et al., 2012, ApJ, 749, L18
Herter T. L. et al., 2013, PASP, 125, 1393
Hill C., Yurchenko S. N., Tennyson J., 2013, Icarus, 226, 1673
Houck J. R. et al., 2004, ApJS, 154, 18
Iłkiewicz K., Mikołajewska J., Stoyanov K., Manousakis S., Miszalski B., 2016, MNRAS, 462, 2695
Ishihara D. et al., 2006, Mem. Soc. Ast. Ital., 77, 1089
Kennea J. A., Mukai K., Sokoloski J. L., Luna G. M. J., Tueller J., Markwardt C. B., Burrows D. N., 2009, ApJ, 701, 1992
Kenyon S. J., Garcia M. R., 1986, AJ, 91, 125
Koike C., Noguchi R., Chihara H., Suto H., Ohtaka O., Imai Y., Matsumoto T., Tsuchiyama A., 2013, ApJ, 778, 60
Luna G. J. M., Sokoloski J. L., Mukai K., 2008, in Evans A., Bode M. F., O'Brien T. J., Darnley M. J., eds, ASP Conf. Ser. Vol. 401, RS Ophiuchi (2006) and the Recurrent Nova Phenomenon. Astron. Soc. Pac., San Francisco, p. 342
Luna G. J. M., Mukai K., Sokoloski J. L., Lucy A., Nelson T., Nu nez N., 2017, Astron. Telegram 10046.
Luna G. J. M. et al., 2018, A&A, 619, A61
Maoz D., Mannucci F., Nelemans G., 2014, ARA&A, 52, 107
Metzger B. D., Hascoët R., Vurm I., Beloborodov A. M. Chomiuk L., Sokoloski J. L., Nelson T., 2014, MNRAS, 442, 713
Metzger B. D., Finzell T., Vurm I., Hascoët R., Beloborodov A. M., Chomiuk L., 2015, MNRAS, 450, 2739
Mukai K., 2008, in Evans A., Bode M. F., O'Brien T. J., Darnley M. J., eds, ASP Conf. Ser. Vol. 401, RS Ophiuchi (2006) and the Recurrent Nova Phenomenon. Astron. Soc. Pac., San Francisco, p. 84
Munari U., Renzini A., 1992, ApJ, 397, L87
Munari U., Moretti S., 2012, Baltic Astron., 21, 22
Munari U. et al., 2011, MNRAS, 410, L52
Munari U. et al., 2012, Baltic Astron., 21, 13
Munari U., Dallaporta S., Cherini G., 2016, New Astron., 47, 7
Munari U., Banerjee D. P. K., 2018, MNRAS, 475, 508
Ness J.-U. et al., 2009, AJ, 137, 3414
Ohnaka K., 2014, A&A, 561, A47
Pan K.-C., Ricker P. M., Taam R. E., 2015, ApJ, 806, 27
Pavlenko Ya. V., 1997, Astron. Rep., 41, 537
Pavlenko Ya. V., 2003, Astron. Rep., 47, 59
Pavlenko Ya. V., Jones H. R. A., Longmore A. J., 2003, MNRAS, 345, 311
Pavlenko Ya. V. et al., 2008, A&A, 485, 541
Pavlenko Ya. V., Woodward C. E., Rushton M. T., Kaminsky B., Evans A., 2010, MNRAS, 404, 206
Pavlenko Ya. V. et al., 2016, MNRAS, 456, 181
Perlmutter S. et al., 1997, ApJ, 483, 565
Perlmutter S. et al., 1999, ApJ, 517, 565
Rayner J. T., Toomey D. W., Onaka P. M., Denault A. J., Stahlberger W. E., Vacca W. D., Cushing M. C., Wang S., 2003, PASP, 115, 362
Riess et al., 1998, AJ, 116, 1009
Rushton M. T. et al., 2014, in Woudt P. A., Riberio V. A. R. M., eds, ASP Conf. Ser. Vol. 490, Stella Novae: Past and Future Decades. Astron. Soc. Pac., San Francisco, p. 249
Schaefer B. E., 2009, ApJ, 697, 721
Schaefer B. E., 2010, ApJS, 187, 275
Schaefer B. E., 2013, Observatory, 133, 81
Schaefer B. E., 2018, MNRAS, 481, 3033
Schafly E. F., Finkbeiner D. P., 2011, ApJ, 737, 103
Schlegel D. J., Finkbeiner D. P., Davis M., 1998, ApJ, 500, 525
Selvelli P. L., Cassatella A., Gilmozzi R., 1992, ApJ, 393, 289
Shahbaz T., Somers M., Yudin B., Naylor T., 1997, MNRAS, 288, 1027
Shara M. M., Prialnik D., Hillman Y., Kovetz A., 2018, ApJ, 860, 110
Sloan G. C., Goes C., Ramirez R. M., Kraemer K. E., Engelke C. W., 2015, ApJ, 811, 45
Starrfield S., 2008, in Evans A., Bode M. F., O'Brien T. J., Darnley M. J., eds, ASP Conf. Ser. Vol. 401, RS Ophiuchi (2006) and the Recurrent Nova Phenomenon. Astron. Soc. Pac., San Francisco, p. 4
Starrfield S., Bose M., Iliadis C., Hix W. R., Wagner R. M., Woodward C. E., José J., Hernanz M., 2019, BAAS, 231, 358.11
Strutskie M. F. et al., 2006, AJ, 131, 1163
Szigeti L. et al., 2018, MNRAS, 474, 4810
Thoroughgood T. D., Dhillon V. S., Littlefair S. P., Marsh T. R., Smith D. A., 2001, MNRAS, 327, 1323
Walder R., Folini D., Shore S. N., 2008, A&A, 484, L9
Werner M. W. et al., 2004, ApJS, 154, 1
Wilson L., 1999, Rep. Prog. Phys., 62, 143
Woodward C. E. et al., 2008, in Evans A., Bode M. F., O'Brien T. J., Darnley M. J., eds, ASP Conf. Ser. Vol. 401, RS Ophiuchi (2006) and the Recurrent Nova Phenomenon. Astron. Soc. Pac., San Francisco, p. 260
Wright E. L. et al., 2010, AJ, 140, 1868
Young E. T. et al., 2012, ApJ, 749, L17
Yudin B., Munari U., 1993, A&A, 270, 165

This paper has been typeset from a TEX/LATEX file prepared by the author.